Received: August 21, 2023. Revised: November 4, 2023. 370

International Journal of
Intelligent Engineering & Systems

http://www.inass.org/

Performance Improvement of Sulselrabar System Using Single-Band Power System Stabilizer Based on Mayfly Algorithm Under Different Loading Condition

Imam Robandi[1]* **Muhammad Ruswandi Djalal[1]** **Mohammad Almas Prakasa[1]**

[1]*Department of Electrical Engineering, Institut Teknologi Sepuluh Nopember, Surabaya 60111, Indonesia*
*Corresponding author's Email: robandi@ee.its.ac.id

Abstract: This study proposes the application of a single-band power system stabilizer type 1A (SB-PSS1A) to enhance the damping ratio in multimachine systems. The mayfly optimization algorithm (MOA) method is employed to optimize the performance of the SB-PSS1A. The South Sulawesi, Southeast Sulawesi, and West Sulawesi regions of the Sulselrabar system are covered by the proposed control plan. To evaluate the effectiveness of the proposed controller, frequency domain analysis and time domain simulation analysis with varying load changes are presented. The accuracy of the MOA method is compared to the swarm intelligence method based on particle swarm optimization (PSO) and firefly algorithm (FA). The analysis results indicate an improvement in system stability, as demonstrated by an increased damping ratio, reduced oscillation overshoot in generator speed and minimum rotor angle, and faster settling time. By implementing SB-PSS1A on 14 generators using the MOA optimization method, a damping ratio of 0.5868 was achieved.

Keywords: Sulselrabar, SB-PSS1A, Mayfly optimization algorithm, Damping, Overshoot.

1. Introduction

Disturbances in the electric power system can arise from transmission breaks or load changes, leading to system instability. This instability encompasses frequency instability, rotor angle deviations, and voltage fluctuations. Instability in the electric power system is influenced by both the initial conditions and the magnitude of the disturbance. These disturbances directly affect changes in electrical power. Electrical power variations have an effect on mechanical power. The difference between the quick response of electrical power and the slower response of mechanical power is one of the elements causing instability. These differences lead to oscillations within the system. The employment of additional equipment, such as the conventional power system stabilizer (PSS), is often used to reduce electrical power oscillations. The PSS dampens the oscillations of the generator, increasing the stability limit. The development of an electric torque component that is in step with the speed changes is referred to as PSS damping.

The application of PSS in multimachine systems demonstrates optimal results in damping oscillations within the power system. Applying PSS1A to a small system or example system results in an increase in system stability. Research [1] presents the stability test of PSS1A under two different uncertainty models on the single machine infinite bus (SMIB) system. In the research study [2, 3], PSS1A is used to improve a two-area, four-engine system's transient stability. Additionally, the IEEE 14-Bus system's stability is increased by using PSS1A and achieving the best parameter optimization [4]. In the 9 bus system connected to the wind turbine, the application of PSS1A has a significant impact on system stability through increasing the system settling time [5]. In previous research [1-5], the system used followed the IEEE example system. To assess the effectiveness of incorporating PSS1A, a more detailed analysis is required, particularly focusing on the dynamics of load changes within large-scale real systems.

The application of PSS1A to real systems has also been carried out by several researchers. In research [6], the implementation of PSS1A in the polish power system, particularly in nuclear power plants, is discussed. This research includes a comparison of the performance of the power system stabilizer PSS1A with that of a predictive control model incorporating additional feedback signals. The findings presented in this paper contribute to the development of a predictive controller model designed to enhance power system stability. In another study, conducted on the 66-Bus New York-New England power system [7], an excellent dynamic response is observed when implementing PSS1A under various power system conditions. The research [6-7] evaluates the performance of PSS1A on large-scale multimachine systems. PSS1A parameters are optimized using heuristic methods and assessed by analyzing critical oscillation modes. However, it's important to note that this research specifically addresses the impact of installing PSS1A when the generator starts operating. Sudden changes in load while the generator is already running also need to be examined, as the controller device will play a crucial role in maintaining system stability in such scenarios.

The South, Southeast, and West Sulawesi (Sulselrabar) system is a multimachine system comprising multiple generators and interconnected large load centers. Over time, the Sulselrabar system has been experiencing growth and expansion. Further studies are required to assess the current and future performance of the Sulselrabar system. Several studies have already been conducted focusing on the stability of the Sulselrabar system [8]. The integration of renewable generators into the Sulselrabar system has also presented stability issues [9]. Currently, there is a need for studies to evaluate the performance of the Sulselrabar system, particularly regarding stability issues. The generator control operation in the Sulselrabar system relies solely on the excitation system without any additional controllers to enhance generator performance. Sudden changes in load on a multimachine system can affect system stability [10].

Optimizing the parameters and locations of PSS is a crucial factor in maximizing their performance. Employing an appropriate optimization method is essential to achieve optimal PSS performance. Currently, the optimization of PSS has been widely explored using various artificial intelligence techniques. For instance, particle swarm optimization (PSO) was employed by [11] for PSS optimization, the Cuckoo search algorithm was used by [12] for PSS optimization in multimachine systems, genetic algorithm was utilized by [13] for PSS tuning in SMIB systems, the cultural algorithm was applied by [14] for PSS optimization, the firefly algorithm was employed by [15] for PSS tuning, and a bio-inspired algorithm was used by [16] for PSS tuning. These studies demonstrate how clever algorithms can be used to achieve the best PSS tuning.

This study utilizes an intelligent optimization technique that is based on the mayfly optimization algorithm (MOA) for PSS optimization. The MOA is based on the PSO algorithm [17] and offers the advantage of combining key features from the PSO algorithm, genetic algorithm (GA) [18], and the firefly algorithm (FA) [19]. The MOA provides a robust hybrid algorithmic framework that draws inspiration from the behavior of the mayfly, incorporates the performance of the PSO algorithm, utilizes crossover techniques [20], and incorporates local search mechanisms [21]. This hybrid approach is employed because it has been demonstrated that the PSO algorithm requires certain modifications to effectively converge to optimal solutions in high-dimensional search spaces [22].

The novelty of this research lies in the use of MOA as a computational method that is fast and precise with an easy structure for optimizing the SB-PSS1A parameters. Furthermore, this study presents an analysis of system reliability for several variations of load changes in the Sulselrabar system. Therefore this research produces a solution to overcome the problem of system stability at various load changes.

This paper is organized into several sections. Section II gives an overview of the Sulselrabar linear model, Section III outlines the research method, Section IV discusses the results of the applied method, and Section V presents the research conclusions.

2. System model

2.1 Generator model

Eq. (1) represents the linear form of the generator, with variations in current, speed, and phase angle serving as the inputs to the equation. v_d and v_q represent the stator voltage components in the d-q axis, v_F denotes the rotor field voltage, v_D and v_Q represent the rotor voltage components in the d-q axis, r represents the stator resistance, L_d and L_q represent the rotor inductance components in the d-q axis, λ_{q0} and λ_{d0} denote the initial flux components in the d-q axis, kMF represents the rotating magnetic field, M_D and M_Q represent the mutual inductance, Δi_d and Δi_q represent the stator current changes in the d-q axis, Δi_F represents the rotor field current change, Δi_D and Δi_Q represent the rotor current changes in the d-q axis,

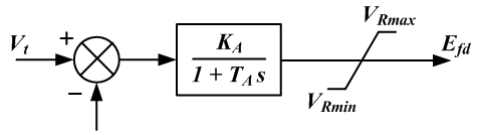

Figure. 1 Exciter model

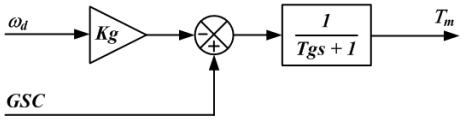

Figure. 2 Governor model

$\Delta\omega$ represents the generator speed change, and $\Delta\delta$ represents the generator rotor angle changes.

$$\begin{bmatrix} \Delta v_d \\ -\Delta v_F \\ 0 \\ \Delta v_q \\ 0 \\ \Delta T_m \\ 0 \end{bmatrix} = - \begin{bmatrix} r & 0 & 0 & \omega_0 L_q & \omega_0 kM_Q & \lambda_{q0} & 0 \\ 0 & rF & 0 & 0 & 0 & 0 & 0 \\ 0 & 0 & rD & 0 & 0 & 0 & 0 \\ -\omega_0 L_d & -\omega_0 kM_F & -\omega_0 kM_D & r & 0 & -\lambda_{d0} & 0 \\ 0 & 0 & 0 & 0 & rQ & 0 & 0 \\ \frac{\lambda_{q0}-L_d i_{q0}}{3} & \frac{-kM_F i_{q0}}{3} & \frac{-kM_D i_{q0}}{3} & \frac{-kM_Q i_{d0}}{3} & \frac{kM_Q i_{d0}}{3} & -D & 0 \\ 0 & 0 & 0 & 0 & 0 & -1 & 0 \end{bmatrix} \begin{bmatrix} \Delta i_d \\ \Delta i_F \\ \Delta i_D \\ \Delta i_q \\ \Delta i_Q \\ \Delta\omega \\ \Delta\delta \end{bmatrix}$$

$$- \begin{bmatrix} L_d & kM_F & kM_D & 0 & 0 & 0 & 0 \\ kM_F & L_F & M_R & 0 & 0 & 0 & 0 \\ kM_D & M_R & L_D & 0 & 0 & 0 & 0 \\ 0 & 0 & 0 & L_q & kM_Q & 0 & 0 \\ 0 & 0 & 0 & kM_Q & L_Q & 0 & 0 \\ 0 & 0 & 0 & 0 & 0 & -\tau_j & 0 \\ 0 & 0 & 0 & 0 & 0 & 0 & 1 \end{bmatrix} \begin{bmatrix} \Delta i_d \\ \Delta i_F \\ \Delta i_D \\ \Delta i_q \\ \Delta i_Q \\ \Delta\dot{\omega} \\ \Delta\delta \end{bmatrix} \quad (1)$$

2.2 Excitation model

A fast exciter is utilized as the exciter type, as illustrated in Figure 1. This specific exciter variant effectively addresses negative damping, which can impede torque attenuation. Eq. (2) [23] presents the formal expression for the fast exciter.

$$E_{fd} = K_A(V_t - V_{ref})/(1 - T_A s) \quad (2)$$

K_A represents the gain, and T_A represents the time constant. To account for equipment limitations, the output of this exciter must be constrained within the range of V_{Rmin} to V_{Rmax}, where V_{Rmin} is the minimum value and V_{Rmax} is the maximum value of the voltage. The block diagram for the fast exciter is depicted in Fig. 1.

2.3 Governor model

Variations in speed, load, and the speed reference all affect how much the governor's mechanical torque (T_m) changes (governor speed changer - GSC). Fig. 2 contains the block diagram illustrative of the governor model [24].

T_m represents the output mechanical torque of the governor, ω_d denotes the generator speed, T_g represents the governor time constant, and K_g is the gain constant, which is equal to 1 divided by R. R represents the droop governor constant. In this governor modeling approach, it is assumed that the GSC is set to 0. The mechanical power produced by the combination of the turbine system and the speed governor can be calculated using Eq. (3).

$$P_m = -\left[\frac{K_g}{1+T_g s}\right]\omega_d \quad (3)$$

K_g, T_g, and R represent the gain constants, governor time constants, and governor droop constants, respectively.

2.4 Test system

The Sulselrabar system links the largest load centers with 16 generators and 46 transmission lines. This system has 37 buses and operates at a voltage of 150 kV. Bus numbering is essential to facilitate the analysis process. Fig. 3 illustrates the single-line diagram of the Sulselrabar system.

2.5 PSS1A

Eq. (4) illustrates the output of the PSS. K_{PSS} represents the PSS gain, T_w represents the washout filter, and T_A, T_B, T_C, and T_D represent the lead-lag gains. Additionally, V_{Smax} and V_{Smin} are the limiters used. The PSS functions by providing an additional signal to the generator excitation. For a visual representation of the conventional single-input PSS1A modeling, refer to Fig. 4.

$$V_s = K_{pss}\frac{T_w s}{1+T_w s}\left[\frac{(1+sT_A)}{(1+sT_B)}\frac{(1+sT_C)}{(1+sT_D)}\right]\omega \quad (4)$$

To process these input signals, transducer and washout circuits are utilized. The transducer is responsible for converting the input signal into a voltage signal, while the washout circuit ensures continuous conditions at the output of the stabilizer.

3. Research method

3.1 Mayfly algorithm

Male and female mayflies are separated into separate flocks. Male mayflies often have stronger bodies, which helps them perform better throughout optimization processes. Eq. (5) illustrates how users of the mayfly algorithm change their places based on their current position I and speed I [25]:

$$P_i(t+1) = P_i(t) + v_i(t+1) \quad (5)$$

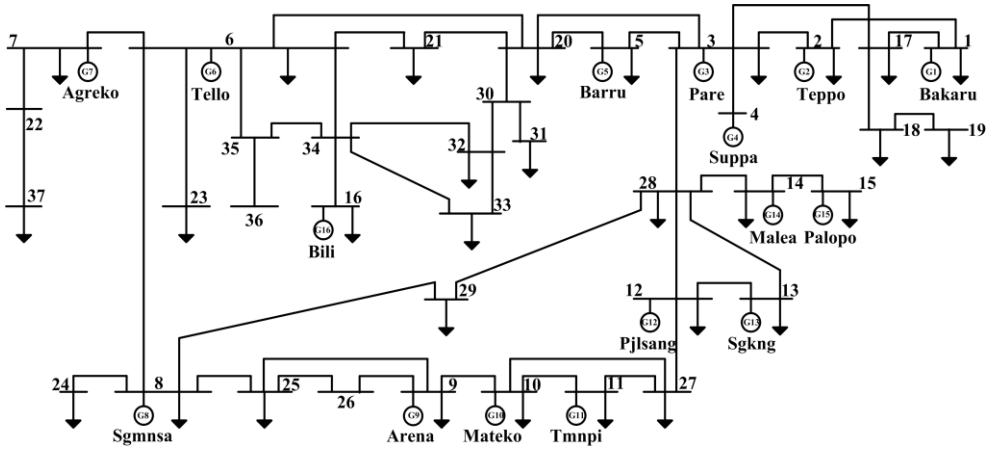

Figure. 3 Sulselrabar system

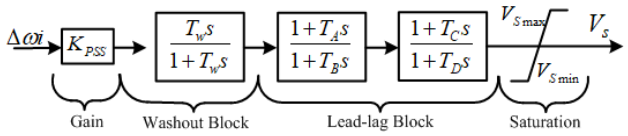

Figure. 4 Block diagram of PSS1A

Male mayfly movements

Based on the most recent fitness value $f(x_i)$ and historically best fitness value on track $f(x_{hi})$ [25], the Speed is updated. Eq. (6) demonstrates how the male mayfly modifies its velocity if $f(x_i) > f(x_{hi})$ depending on its present velocity, the distance between it and the best global position, and the best historical trajectory.

$$v_i(t+1) = g.v_i(t) + a_i e^{-\beta r_p^2}[x_{hi} - x_i(t)] + a_2 e^{-\beta r_g^2}[x_g - x_i(t)] \quad (6)$$

g is a variable that linearly descends from the maximum to the minimum value. a_1, a_2, and β are constants used to balance the weights. The variables r_p and r_g are utilized to determine the Cartesian separation between individuals and their historically optimal swarm placements. The second norm for distance arrays will be Cartesian space [25]:

$$\left||x_i - x_j|\right| = \sqrt{\sum_{k=1}^{n}(x_{ik} - x_{jk})^2} \quad (7)$$

The male mayfly will change its speed from its present speed using a random dance coefficient d if $f(x_i) < f(x_{hi})$:

$$v_i(t+1) = g.v_i(t) + d.r_i \quad (8)$$

r_i is a uniformly distributed random number that is selected from the range [-1, 1] in this instance.

Female mayfly movements

The female mayfly uses a different technique to increase its speed. Winged female mayflies have a lifespan of one to seven days according to biology, during which time they actively look for male mayflies to mate with and breed with. As a result, depending on the chosen male mayfly, the female mayflies alter their speed [25].

The first couple will be the best male and female mayflies, and so on. So if $f(y_i) < f(x_i)$ for the i-th female mayfly:

$$v_i(t+1) = g.v_i(t) + a_3 e^{-\beta r_{mf}^2}[x_i(t) - y_i(t)] \quad (9)$$

Another constant that is used to balance speed is a_3. The Cartesian distance between them is represented by the number r_m.

In contrast, if $(y_i) < f(x_i)$, the female mayfly renews its speed by performing another arbitrary dance fl. A random number in the range [-1, 1] is called r_2.

$$v_i(t) = g.v_i(t) + fl.r_2 \quad (10)$$

3.2 The MOA implementation

The resulting mathematical model is converted into a state space representation, as illustrated in Eqs. (11) and (12).

$$\Delta\dot{x} = A\Delta x + B\Delta u \quad (11)$$

$$\Delta y = C\Delta x + D\Delta u \quad (12)$$

The assessment of system stability can be determined by analyzing Matrix A using Eq. (13).

Table 1. Parameters

Methods	Parameters	Values
PSO	Particles	30
	Social (C_2) & Cognitive (C_1) Const.	2
	The quantity of variables	8
	W Inersia Moment	0.9
FA	Alpha; Beta; Gamma	0.25; 0.2; 1;
	Dimension	80
MOA	Population Size	20
	Global Learning (a_2, a_3)	1.5
	Distance sight (Beta)	2
	Inertia Weight	0.8
	Damping, Random flight	1
	Dance of the Nuptials	5
	Offsprings; Mutants	20; *round(0.05*n_{Pop})*;
	Dance_Damp; Mating; Mutation	0.8; 0.99; 0.01;

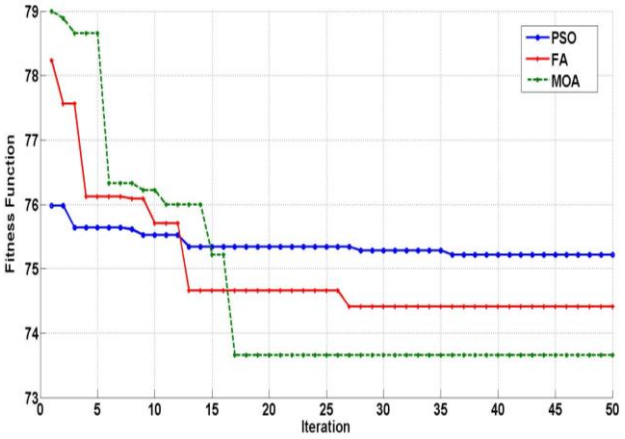

Figure. 5 Convergence graphic

$$\det(sI-A)=0 \tag{13}$$

The identity matrix *(I)* and eigenvalues *(s)* of matrix *A* are utilized in the analysis. Matrix *A* has dimensions of *n x n*. The number of eigenvalue systems can be calculated using Eq. (14).

$$\lambda_i = \sigma_i + j\omega_i \tag{14}$$

$$f = \frac{\omega}{2\pi} \tag{15}$$

Eq. (15) represents the oscillation frequency. In the equation, λ_i denotes the eigenvalue, σ_i represents the real component of the eigenvalue, and ω_i signifies the imaginary component of the eigenvalue. The system's damping component is represented in the real eigenvalue section, while the oscillation component is depicted in the imaginary eigenvalue section. Eq. (16) provides the calculation for the damping value. The comprehensive damping index (CDI), illustrated in Eq. (17), offers an assessment of the system's overall damping.

$$\zeta_i = \frac{-\sigma_i}{\sqrt{\sigma_i^2+\omega_i^2}} \tag{16}$$

$$CDI = \sum_{i=1}^{n}(1-\zeta_i) \tag{17}$$

The system's damping ratio is denoted as ζ_i, while the sum of the eigenvalues is represented by *n*. The primary function of MOA is to maximize the minimum damping (ζ_{min}). The parameter limits of SB-PSS1A optimized using MOA are $K_{pss(min)} \leq K_{pss} \leq K_{pss(max)}$; $T_{1(min)} \leq T_1 \leq T_{1(max)}$; $T_{2(min)} \leq T_2 \leq T_{2(max)}$; $T_{3(min)} \leq T_3 \leq T_{3(max)}$; *and* $T_{4(min)} \leq T_4 \leq T_{4(max)}$.

Fig. 5 displays the convergence graph for the MOA computational method, demonstrating that MOA outperforms PSO and FA in terms of optimization results. Specifically, MOA achieves the smallest fitness function value of 73.3655 and converges at the 17th iteration, whereas PSO attains a fitness function value of 75.2189 at the 36th iteration, and FA reaches 74.4102 at the 27th iteration. Thus, MOA exhibits more efficient performance compared to PSO and FA. The MOA parameters utilized in this analysis are provided in Table 1.

4. Results and discussion

This section aims to enhance the stability of the Sulselrabar system by implementing SB-PSS1A equipment. The simulation employs a system model with two configurations: without and with SB-PSS1A. To evaluate the performance of the MOA optimization, this research compares it with the PSO and FA algorithm. The objective function is designed to maximize the minimum damping ratio (ζ_{min}). The analytical methods employed in this study include damping analysis and time domain simulation. Damping analysis involves observing the damping value associated with each SB-PSS1A installation option, while time domain simulation evaluates

Table 2. Tuning results of the PSS

G	PSO					FA				
	K_{pss}	T_1	T_2	T_3	T_4	K_{pss}	T_1	T_2	T_3	T_4
1	48	0.0461	0.8240	0.0474	0.0877	47.3114	0.0593	0.8034	0.0422	0.0852
2	17	0.0438	0.2791	0.3549	1.4569	16.6528	0.0400	0.3000	0.3867	1.4000
3	13.7395	0.0528	0.3194	0.1567	2.7507	13.3737	0.0568	0.3677	0.1269	2.7000
4	16	0.0529	0.7852	0.1888	1.6935	15.8254	0.0437	0.7000	0.1365	1.6000
5	47	0.0406	0.2999	0.1217	2.1436	46.4846	0.0495	0.2000	0.1573	2.1191
6	35.5540	0.0518	0.3561	0.1612	1.4757	35.8690	0.0461	0.3267	0.2000	1.4580
7	29	0.0532	0.0837	0.1219	1.4414	29.6088	0.0600	0.0900	0.1943	1.4294
8	40	0.0414	0.0199	0.1765	1.7777	39.8460	0.0400	0.0100	0.1566	1.7359
9	30	0.0576	0.7639	0.1731	1.5407	29.0361	0.0400	0.7000	0.1109	1.5000
10	100	0.0542	0.9450	0.1677	2.8351	99.4360	0.0583	0.9239	0.1629	2.8000
11	97.7148	0.0502	0.9744	0.1467	0.1889	97.8932	0.0600	0.9012	0.2000	0.1000
12	8.2085	0.0564	0.2248	0.4254	0.8050	8.3029	0.0600	0.2638	0.4000	0.8693
13	78	0.0411	0.1381	0.3206	1.9485	78.3375	0.0534	0.1400	0.3950	1.9401
14	17.8569	0.0453	0.3546	0.0156	0.5810	17.4993	0.0427	0.3509	0.0140	0.5000

G	MOA				
	K_{pss}	T_1	T_2	T_3	T_4
1	47.8350	0.0600	0.8839	0.0402	0.0804
2	16.0000	0.0489	0.2218	0.3674	1.4671
3	14.0000	0.0600	0.4000	0.1000	2.7118
4	15.2509	0.0600	0.7729	0.2000	1.7000
5	47.0000	0.0536	0.2000	0.1474	2.1766
6	35.0000	0.0460	0.3998	0.1000	1.4000
7	29.0000	0.0534	0.0800	0.2000	1.4402
8	39.0000	0.0494	0.0100	0.2000	1.7000
9	30.0000	0.0600	0.7244	0.2000	1.5003
10	99.0700	0.0400	0.9151	0.1000	2.8313
11	98.0000	0.0400	0.9000	0.1648	0.1000
12	8.7365	0.0400	0.2000	0.5000	0.8653
13	78.1089	0.0409	0.1400	0.3075	1.9905
14	17.0986	0.0484	0.3552	0.0114	0.6000

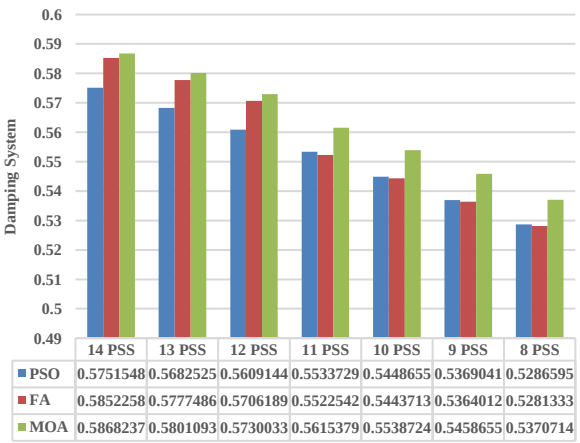

Figure. 6 Placement index damping system

system performance by analyzing the responses of deviation speed *(Δω)*, field voltage *(E_{fd})*, and rotor angle for each generator.

4.1 Damping analysis

In Fig. 6, the Placement Index for each SB-PSS1A installation scheme is depicted. The addition of SB-PSS1A results in increased damping, particularly for systems equipped with 14 SB-PSS1A. The maximum damping ratio is achieved as follows: using 14 SB-PSS1A with MOA results in a damping value of 0.5868, while with PSO, it is 0.5751, and with FA, it is 0.5852. For a system to be considered stable and capable of dampening system oscillations, a desirable damping value should exceed 0.1. The tuning results for the SB-PSS1A parameters can be found in Table 2.

4.2 Time domain simulation

This section focuses on evaluating the stability of the system by analyzing the response of speed deviation, field voltage, and rotor angle for each generator. Additionally, the response of the TELLO LAMA (TL) generator during a disturbance is examined in this section. To investigate the dynamic performance of the generator's response, the system is subjected to disturbances in the form of variations in load changes.

Table 3. Generator speed overshoot response

G	No PSS (pu)	PSS1A PSO (pu)	PSS1A FA (pu)	PSS1A MOA (pu)
1	-0.021 & 0.0032	-0.017 & 0.002	-0.017 & 0.001	-0.015 & 0.0005
2	-0.019 & 0.005	-0.017 & 0.004	-0.017 & 0.003	-0.015 & 0.001
3	-0.019 & 0.003	-0.018 & 0.002	-0.018 & 0.002	-0.016 & 0.001
4	-0.019 & 0.004	-0.018 & 0.004	-0.018 & 0.004	-0.018 & 0.002
5	-0.095 & 0.03	-0.079 & 0.02	-0.074 & 0.02	-0.051 & 8.7e-05
6	-0.210 & 0.054	-0.207 & 0.052	-0.207 & 0.051	-0.205 & 0.047
7	-0.224 & 0.091	-0.174 & 0.032	-0.167 & 0.0204	-0.148 & 0.00017
8	-0.056 & 0.008	-0.049 & 0.002	-0.048 & 0.001	-0.040 & 1.9e-05
9	-0.023 & 0.005	-0.021 & 0.003	-0.021 & 0.003	-0.020 & 0.002
10	-0.021 & 0.008	-0.019 & 0.006	-0.019 & 0.006	-0.016 & 0.004
11	-0.022 & 0.015	-0.020 & 0.013	-0.020 & 0.013	-0.018 & 0.008
12	-0.020 & 0.009	-0.016 & 0.004	-0.015 & 0.003	-0.016 & 0.003
13	-0.024 & 0.004	-0.021 & 0.003	-0.022 & 0.003	-0.015 & 0.001
14	-0.019 & 0.013	-0.016 & 0.010	-0.016 & 0.009	-0.015 & 0.006
15	-0.020 & 0.015	-0.017 & 0.012	-0.017 & 0.012	-0.015 & 0.007
16	-0.068 & 0.016	-0.063 & 0.011	-0.062 & 0.010	-0.058 & 0.005

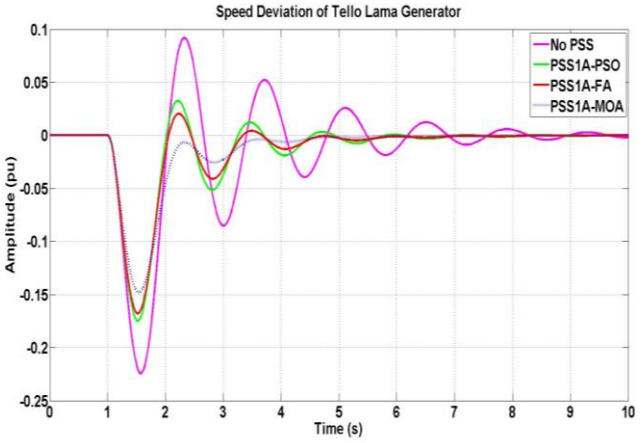

Figure. 7 Speed deviation (Δω) of TL generator

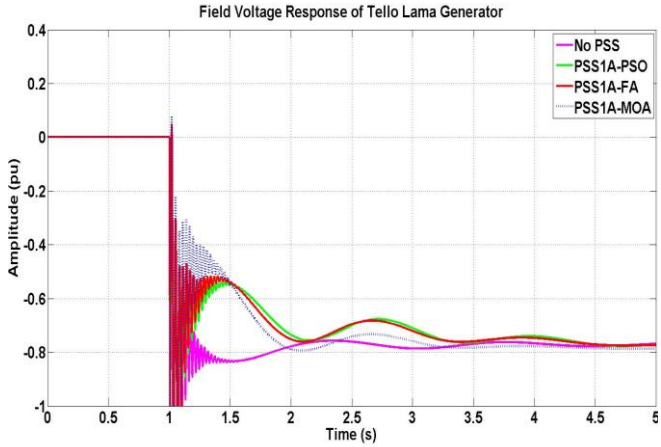

Figure. 8 Field voltage response (E_{fd}) of TL generator

4.2.1. Case study 1

The first case study focused on investigating the dynamic response of the generator to a small disturbance applied to the TL bus load, specifically a 0.5 pu input step change in load. Fig. 7 compares the speed response of the generator in two scenarios: without and with SB-PSS1A. The system without SB-PSS1A displays significant oscillations, ranging from -0.224 to 0.091 pu. The proposed MOA-based tuning method demonstrates an improvement in the stability of generator speed. After the installation of additional controls with SB-PSS1A, there was an improvement in system stability. The MOA-based SB-PSS1A tuning provides the most optimal speed response results, as indicated by the minimum overshoot ranging from -0.148 to 0.00017 pu. On the other hand, utilizing SB-PSS1A based on PSO results in an overshoot ranging from -0.174 to 0.032 pu, while using FA results in a range of -0.167 to 0.0204 pu.

Table 3 shows that the minimum overshoot deviation is observed in a system with a control scheme based on SB-PSS1A, which is optimized using MOA, compared to the control scheme based on PSO and FA. The generator performance is indeed significantly improved with the installation of a SB-PSS1A. The SB-PSS1A equipment enhances the generator's performance by providing an additional control signal, specifically the field voltage.

Fig. 8 showcase the field voltage response of the TL generator during a disturbance, providing a visual demonstration of the effectiveness of the SB-PSS1A in stabilizing the generator's operation. The generators equipped with SB-PSS1A exhibit a more pronounced additional signal compared to those without SB-PSS1A. In addition, Table 4 presents the field voltage overshoot response for each control scheme.

Table 4. Field voltage generator response (E_{fd})

G	No PSS (pu)	PSS1A PSO (pu)	PSS1A FA (pu)	PSS1A MOA (pu)
1	-0.034 & 0.017	-0.034 & 0.023	-0.034 & 0.023	-0.033 & 0.026
2	-0.026 & 0.007	-0.026 & 0.005	-0.026 & 0.004	-0.022 & 0.016
3	-0.051 & 0.001	-0.051 & 0.001	-0.051 & 0.003	-0.060 & 0.019
4	-0.041 & 0.003	-0.041 & 0.001	-0.041 & 0.002	-0.042 & 0.007
5	-0.13 & 1.9e-29	-0.13 & 2.5e-30	-0.13 & 1.9e-29	-0.12 & 1.9e-29
6	-1 & 3e-29	-1 & 3e-29	-1 & 3e-29	-1 & 3e-29
7	-1 & 0.0313	-1 & 0.0422	-1 & 0.0487	-1 & 0.0796
8	-2.56 & 2.5e-29	-2.46 & 3.4e-30	-2.444 & 2.5e-29	-2.116 & 2.5e-29
9	-0.191 & 0.121	-0.190 & 0.114	-0.191 & 0.113	-0.191 & 0.082
10	-0.044 & 0.056	-0.019 & 0.006	-0.019 & 0.006	-0.016 & 0.004
11	-0.022 & 0.016	-0.020 & 0.013	-0.020 & 0.013	-0.018 & 0.008
12	-0.031 & 0.018	-0.016 & 0.004	-0.015 & 0.003	-0.016 & 0.003
13	-0.028 & 5e-27	-0.021 & 0.003	-0.022 & 0.003	-0.015 & 0.001
14	-0.019 & 0.002	-0.016 & 0.010	-0.016 & 0.009	-0.015 & 0.006
15	-0.003 & 0.005	-0.017 & 0.012	-0.017 & 0.012	-0.015 & 0.007
16	-0.5649 & 0	-0.5608 & 0	-0.5588 & 0	-0.5489 & 0

Table 5. Rotor angle settling time response

G	No PSS (s)	PSS1A PSO (s)	PSS1A FA (s)	PSS1A MOA (s)
1	13.13	10.42	7.99	6.55
2	13.67	10.48	8.53	6.91
3	13.19	10.32	9.52	6.80
4	13.89	10.66	8.32	6.93
5	11.14	10.19	8.25	6.42
6	8.168	7.247	6.82	6.40
7	11.58	6.79	6.22	5.48
8	9.494	7.09	6.42	4.88
9	11.83	9.44	8.36	7.47
10	15.59	12.37	10.07	8.64
11	16.71	13.57	11.01	7.75
12	16.76	13.54	11.45	8.19
13	14.65	11.46	9.97	6.5
14	19.23	16.67	14.77	9.52
15	15.74	14.26	13.91	9.84
16	8.61	7.63	6.55	6.17

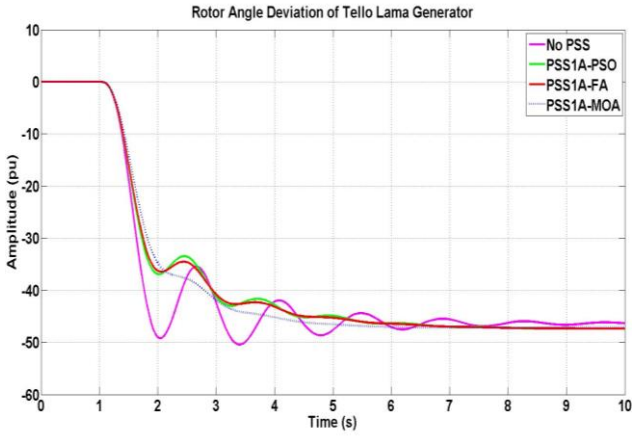

Figure. 9 Rotor angle deviation of TL generator

Fig. 9 display the Rotor Angle deviation response of the TL generators. The generator without additional control exhibits more oscillations and a longer settling time compared to the generator with additional control. These figures provide visual evidence of the improved stability achieved through the implementation of additional control measures.

The TL generator has a settling time of 11.58 seconds without additional control. By using the proposed MOA-based optimization method, a settling time of 5.48s is achieved with SB-PSS1A. Meanwhile, the settling time using PSO is 6.79 seconds, while with FA, it is 6.22 seconds. Table 5 provides a comparison of the settling times for the generators under different control schemes.

4.2.2. Case study 2

In the second case study, we utilize a case study involving the first load change variation at 0 seconds, followed by the second variation which occurs at 10 seconds. The first load change value is 0.5 pu,

Table 6. Generator speed overshoot response

G	No PSS (pu)		PSS1A PSO (pu)	
	LV 1	LV 2	LV 1	LV 2
1	-0.0212 & 0.0032	-0.0016 & 0.0006	-0.0176 & 0.0022	-0.0013 & 0.0004
2	-0.0190 & 0.0053	-0.0013 & 0.0008	-0.0173 & 0.0040	-0.0012 & 0.0006
3	-0.0194 & 0.0031	-0.0013 & 0.0004	-0.0185 & 0.0027	-0.0012 & 0.0004
4	-0.0191 & 0.0045	-0.0013 & 0.0007	-0.0181 & 0.0044	-0.0013 & 0.0006
5	-0.0954 & 0.0386	-0.0057 & 0.0036	-0.0783 & 0.0294	-0.0057 & 0.0036
6	-0.2105 & 0.0544	-0.0027 & 0.0024	-0.2079 & 0.0500	-0.0022 & 0.0021
7	-0.2227 & 0.0906	-0.0455 & 0.0315	-0.1745 & 0.0318	-0.0392 & 0.0202
8	-0.0562 & 0.0077	-0.0038 & 0.0019	-0.0488 & 0.0014	-0.0034 & 0.0014
9	-0.0235 & 0.0055	-0.0014 & 0.0008	-0.0219 & 0.0034	-0.0013 & 0.0005
10	-0.0212 & 0.0084	-0.0013 & 0.0010	-0.0195 & 0.0066	-0.0011 & 0.0006
11	-0.0219 & 0.0150	-0.0016 & 0.0015	-0.0203 & 0.0127	-0.0012 & 0.0010
12	-0.0204 & 0.0094	-0.0014 & 0.0011	-0.0161 & 0.0047	-0.0011 & 0.0005
13	-0.0240 & 0.0045	-0.0017 & 0.0009	-0.0215 & 0.0033	-0.0016 & 0.0006
14	-0.0197 & 0.0138	-0.0023 & 0.0021	-0.0168 & 0.0103	-0.0018 & 0.0014
15	-0.0199 & 0.0153	-0.0027 & 0.0024	-0.0179 & 0.0128	-0.0020 & 0.0017
16	-0.0680 & 0.0162	-0.0047 & 0.0028	-0.0628 & 0.0115	-0.0040 & 0.0023
G	**PSS1A FA (pu)**		**PSS1A MOA (pu)**	
	LV 1	**LV 2**	**LV 1**	**LV 2**
1	-0.0173 & 0.0016	-0.0013 & 0.0004	-0.0155 & 0.0001	-0.0009 & 0.0001
2	-0.0172 & 0.0039	-0.0011 & 0.0005	-0.0151 & 0.0010	-0.0008 & 0.0002
3	-0.0183 & 0.0025	-0.0014 & 0.0004	-0.0161 & 0.0010	-0.0011 & 0.0003
4	-0.0188 & 0.0047	-0.0012 & 0.0006	-0.0184 & 0.0024	-0.0010 & 0.0004
5	-0.0745 & 0.0194	-0.0043 & 0.0024	-0.0512 & 0	-0.0025 & 0.0002
6	-0.2075 & 0.0492	-0.0022 & 0.0019	-0.2032 & 0.0470	-0.0020 & 0.0015
7	-0.1664 & 0.0204	-0.0379 & 0.0167	-0.1466 & 0	-0.0332 & 0.0106
8	-0.0483 & 0.0012	-0.0031 & 0.0014	-0.0401 & 0	-0.0027 & 0.0001
9	-0.0216 & 0.0035	-0.0013 & 0.0004	-0.0205 & 0.0021	-0.0012 & 0.0003
10	-0.0195 & 0.0068	-0.0011 & 0.0006	-0.0166 & 0.0041	-0.0008 & 0.0001
11	-0.0203 & 0.0131	-0.0014 & 0.0012	-0.0181 & 0.0085	-0.0008 & 0.0004
12	-0.0151 & 0.0035	-0.0010 & 0.0004	-0.0162 & 0.0038	-0.0008 & 0.0002
13	-0.0222 & 0.0036	-0.0016 & 0.0006	-0.0155 & 0.0012	-0.0008 & 1.09e-05
14	-0.0165 & 0.0097	-0.0017 & 0.0014	-0.0154 & 0.0068	-0.0007 & 0.0003
15	-0.0174 & 0.0124	-0.0022 & 0.0017	-0.0151 & 0.0073	-0.0007 & 0.0003
16	-0.0623 & 0.0103	-0.0042 & 0.0020	-0.0579 & 0.0049	-0.0037 & 0.0011

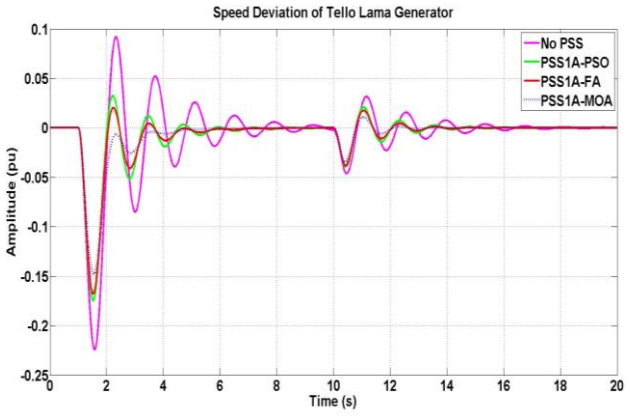

Figure. 10 Speed deviation (Δω) of TL generator

equivalent to 50 MW, while the second load change value is 1 pu, equivalent to 100 MW.

Fig. 10 depicts the speed response of the TL generator. Without SB-PSS1A, the generator speed response exhibited oscillations and overshoot during the first load variation (LV), ranging from -0.2227 to 0.0906 pu, and during the second load variation, ranging from -0.0455 to 0.0315 pu. Upon implementing SB-PSS1A with PSO optimization, the overshoot is reduced to -0.1745 to 0.0318 pu for the first load variation and -0.0392 to 0.0202 pu for the second load variation. Subsequently, the FA-based SB-PSS1A produces an overshoot of -0.1664 to 0.0204 pu in the first load variation and -0.0379 to 0.0167 pu in the second load variation. Utilizing SB-PSS1A with MOA optimization yielded even lower overshoot values: -0.1473 to 0 pu for the first load variation and -0.03197 to 0.01039 pu for the second load variation. For a comprehensive overview of the overshoot oscillation speed response data for each generator, please refer to Table 6.

Table 7. Comparison of field voltage response (E_{fd})

G	No PSS (pu)		PSS1A PSO (pu)	
	LV 1	LV 2	LV 1	LV 2
1	-0.0358 & 0.0165	-0.0145 & 0.0135	-0.0369 & 0.0230	-0.0191 & 0.0205
2	-0.0267 & 0.007	-0.0019 & 0.0031	-0.0268 & 0.0051	-0.0015 & 0.0034
3	-0.0514 & 0.0016	-0.0093 & -0.0014	-0.0512 & 0.0028	-0.0071 & -0.0006
4	-0.0414 & 0.0036	-0.0084 & -0.0011	-0.0414 & -0.0017	-0.0083 & -0.0008
5	-0.1371 & -0.1104	-0.1279 & -0.1171	-0.1344 & -0.0853	-0.131 & -0.1155
6	-0.00009 & -1	-0.00009 & -1	-0.00009 & -1	-0.00009 & -1
7	0.0610 & -1	0.0182 & -1	-0.0736 & -1	0.3417 & -1
8	-2.56 & -0.9968	-1.198 & -0.8747	-2.458 & -0.9797	-1.19 & -0.8021
9	-0.1913 & 0.1243	-0.0550 & 0.0423	-0.1898 & 0.1185	-0.0680 & 0.0568
10	-0.045 & 0.0528	-0.0325 & 0.0233	-0.0194 & 0.0065	-0.0012 & 0.0006
11	-0.0200 & 0.0166	-0.0101 & 0.0113	-0.0205 & 0.0129	-0.0013 & 0.0010
12	-0.0317 & 0.0164	-0.0215 & 0.0048	-0.0162 & 0.0047	-0.0011 & 0.0006
13	-0.0280 & -0.0153	-0.0228 & -0.0166	-0.0215 & 0.0033	-0.0016 & 0.0006
14	-0.0199 & 0.0012	-0.0148 & -0.0026	-0.0168 & 0.0103	-0.0017 & 0.0014
15	-0.0041 & 0.0053	-0.0028 & 0.0014	-0.0179 & 0.0127	-0.0019 & 0.0017
16	-0.5637 & -0.2368	-0.2809 & -0.1996	-0.5623 & -0.2375	-0.2792 & -0.1778
G	**PSS1A FA (pu)**		**PSS1A MOA (pu)**	
	LV 1	**LV 2**	**LV 1**	**LV 2**
1	-0.0355 & 0.0227	-0.0171 & 0.0207	-0.0350 & 0.0276	-0.0212 & 0.0249
2	-0.0268 & 0.004	-0.0016 & 0.0036	-0.0221 & 0.0163	-0.0015 & 0.0052
3	-0.0513 & 0.003	-0.007 & -0.0009	-0.06 & 0.0195	-0.0091 & -0.0012
4	-0.0412 & 0.0021	-0.008 & -0.0005	-0.0426 & 0.0078	-0.0081 & -0.0005
5	-0.133 & -0.0786	-0.1308 & -0.113	-0.1275 & -0.0438	-0.128 & -0.1071
6	-0.00009 & -1	-0.00009 & -1	-0.00009 & -1	-0.00009 & -1
7	0.0815 & -1	0.4211 & -1	0.1178 & -1	0.6895 & -1
8	-2.439 & -0.978	-1.19 & -0.7874	-2.117 & -0.3964	-1.167 & -0.7434
9	-0.1907 & 0.1173	-0.0735 & 0.0610	-0.1879 & 0.0862	-0.0837 & 0.0717
10	-0.0194 & 0.0068	-0.0012 & 0.0006	-0.0167 & 0.0042	-0.0007 & 0.0001
11	-0.0206 & 0.0133	-0.0014 & 0.0012	-0.0181 & 0.0084	-0.0008 & 0.0004
12	-0.0151 & 0.0037	-0.0010 & 0.0004	-0.0162 & 0.0038	-0.0007 & 0.0002
13	-0.0222 & 0.0035	-0.0016 & 0.0006	-0.0155 & 0.0012	-0.0008 & 5.8e-05
14	-0.0165 & 0.0098	-0.0018 & 0.0014	-0.0154 & 0.0068	-0.0007 & 0.0003
15	-0.0176 & 0.0125	-0.0022 & 0.0017	-0.0153 & 0.0074	-0.0007 & 0.0003
16	-0.5673 & -0.237	-0.2904 & -0.172	-0.5503 & -0.2374	-0.305 & -0.1587

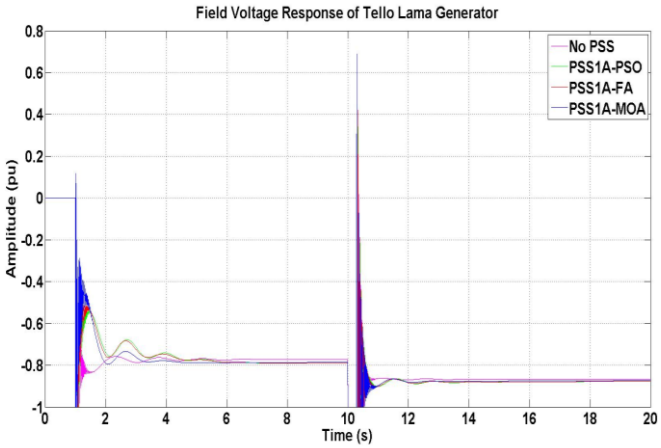

Figure. 11 Field voltage response (E_{fd}) of TL generator

Fig. 11 illustrates the field voltage response of the TL generator in the presence of different load changes. Analyzing the graph of the field voltage generator response reveals the effectiveness of the PSS response in supplying additional control signals during load variations. The oscillation overshoot of the field voltage response for each generator is detailed in Table 7.

Fig. 12 shows the rotor angle response of the TL generator during various load changes. The graph of the rotor angle response shows that the optimal performance with the MOA-based SB-PSS1A is indicated by the fast settling time. Table 8 shows the settling time response of each generator in the two case studies of variations in load changes.

PSS equipment not only enhances stability but also provides additional signals to the generator. It effectively addresses the dynamics of load changes when the exciter alone may not be sufficient, particularly in large-scale power systems that necessitate optimal coordination. In this study, the SB-PSS1A parameters were optimized using the

Table 8. Rotor angle settling time response

G	No PSS (s)		PSS1A PSO (s)		PSS1A FA (s)		PSS1A MOA (s)	
	LV1	LV2	LV1	LV2	LV1	LV2	LV1	LV2
1	>10	14.26	>10	12.51	>10	12.17	6.10	11.75
2	>10	15.69	>10	13.61	>10	12.49	6.48	11.63
3	>10	15.03	>10	13.62	>10	13.37	6.36	11.43
4	>10	15.51	>10	13.94	>10	13.46	6.43	12.01
5	>10	15.27	8.55	13.29	8.26	12.63	5.30	11.35
6	6.80	13.07	6.62	12.72	6.40	12.41	6.02	12.28
7	>10	>20	6.81	13.92	7.41	13.59	5.22	12.54
8	6.39	14.39	5.51	12.75	5.16	12.48	4.09	11.45
9	>10	17.11	>10	14.49	>10	14.04	6.54	11.74
10	>10	17.2	>10	15.54	>10	14.76	6.60	12.46
11	>10	17.02	>10	15.53	>10	14.83	7.69	13.11
12	>10	16.07	>10	14.48	>10	13.05	7.45	12.27
13	>10	16.19	>10	13.44	>10	13.11	6.58	11.42
14	>10	18.66	>10	17.68	>10	16.36	8.92	13.29
15	>10	19.04	>10	17.17	>10	16.24	9.26	12.82
16	7.98	15.28	6.89	14.13	6.86	13.92	5.53	13.79

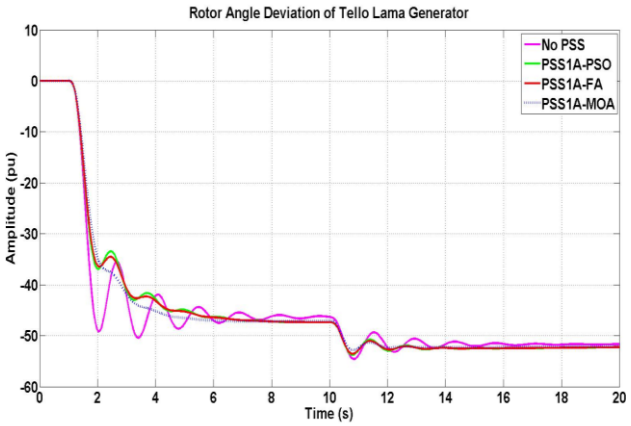

Figure. 12 Rotor angle deviation of TL generator

MOA algorithm. The optimization results demonstrate that the MOA algorithm outperforms PSO in terms of achieving the same objective function. The MOA optimization process is faster in finding the optimal SB-PSS1A parameters. When the SB-PSS1A parameters are precisely tuned, it leads to optimal generator performance. The improved stability of the Sulselrabar system is evident through the reduction of overshoot oscillations and faster settling time following the installation of SB-PSS1A. Particularly, the implementation of SB-PSS1A contributes to maximum damping of the system, further enhancing its stability. These improvements signify the effectiveness of SB-PSS1A in optimizing the system's response and mitigating oscillations.

5. Conclusion

This study aims to enhance the stability of the Sulselrabar electrical system through the utilization of SB-PSS1A. To achieve optimal performance of SB-PSS1A, the MOA-based optimization method is employed to optimize its parameters. The improvement in stability is evidenced by an increase in the system's damping ratio, reduction in the overshoot of oscillation responses in generator speed and rotor angle, as well as faster settling time. The implementation of SB-PSS1A on 14 generators using the MOA optimization method resulted in a damping ratio of 0.5868. In future research, the SB-PSS1A control scheme can be further explored by integrating it with solar and wind energy systems to enhance the overall efficiency and sustainability of the electrical system.

Conflicts of interest

The authors declare no conflict of interest.

Author contributions

Conceptualization, Imam Robandi, Muhammad Ruswandi Djalal, Mohammad Almas Prakasa; methodology, Imam Robandi and Muhammad Ruswandi Djalal; software, Muhammad Ruswandi Djalal; Validation, Imam Robandi and Muhammad Ruswandi Djalal; formal analysis, Muhammad Ruswandi Djalal and Muhammad Almas Prakasa; investigation, Imam Robandi and Muhammad Ruswandi Djalal; resources, Muhammad Ruswandi Djalal; writing original draft preparation, Muhammad Ruswandi Djalal; writing review and editing, Mohammad Almas Prakasa; visualization, Muhammad Ruswandi Djalal, All authors have read and agreed to the published version of the manuscript.

Acknowledgments

The authors would like to thank the National Research and Innovation Agency (BRIN) and the Education Fund Management Institute (LPDP) for providing funding for this research.

References

[1] L. A. O. Padilla, R. P. Gallardo, and J. A. M. Saldaña, "Robust stability analysis for a power system stabilizer", In: *Proc. of 2016 13th International Conference on Power Electronics (CIEP)*, pp. 345-349, 2016, doi: 10.1109/CIEP.2016.7530782.

[2] A. A. Alsakati, C. A. Vaithilingam, K. Naidu, G. Rajendran, J. Alnasseir, and A. Jagadeeshwaran, "Particle Swarm Optimization for Tuning Power System Stabilizer towards Transient Stability Improvement in Power System Network", In: *Proc. of 2021 IEEE International Conference on Artificial Intelligence in Engineering and Technology (IICAIET)*, pp. 1-6, 2021, doi: 10.1109/IICAIET51634.2021.9573534.

[3] M. Zarifakis, W. T. Coffey, Y. P. Kalmykov, S. V. Titov, D. J. Byrne, and S. J. Carrig, "Active Damping of Power Oscillations Following Frequency Changes in Low Inertia Power Systems", *IEEE Transactions on Power Systems*, Vol. 34, No. 6, pp. 4984-4992, 2019, doi: 10.1109/TPWRS.2019.2911845.

[4] P. Marić, R. Kljajić, H. R. Chamorro, and H. Glavaš, "Power system stabilizer tuning algorithm in a multimachine system based on s-domain and time domain system performance measures", *Energies*, Vol. 14, No. 18, p. 5644, 2021, doi: 10.3390/en14185644.

[5] A. A. Alsakati, C. A. Vaithilingam, B. Ramlochun, and A. Khujaev, "Power System Stabilizer for Stability Enhancement of Wind Generators Connected to Power System", In: *Proc. of 2021 IEEE 19th Student Conference on Research and Development (SCOReD)*, pp. 245-250, 2021, doi: 10.1109/SCOReD53546.2021.9652739.

[6] P. Sokólski, T. A. Rutkowski, B. Ceran, D. Horla, and D. Złotecka, "Power system stabilizer as a part of a generator MPC adaptive predictive control system", *Energies*, Vol. 14, No. 20, p. 6631, 2021.

[7] O. José and C. Jaime, "Power System Stabilizer Adaptive Tuning Based on Decision Trees and a Heuristic Optimization Process", *Revista Politécnica*, Vol. 51, No. 1, pp. 57-66, 2023, doi: 10.33333/rp.vol51n1.05.

[8] M. R. Djalal, A. Imran, and I. Robandi, "Optimal placement and tuning power system stabilizer using Participation Factor and Imperialist Competitive Algorithm in 150 kV South of Sulawesi system", In: *Proc. of 2015 International Seminar on Intelligent Technology and Its Applications (ISITIA)*, pp. 147-152, 2015, doi: 10.1109/ISITIA.2015.7219970.

[9] A. Siswanto, I. C. Gunadin, S. M. Said, and A. Suyuti, "Stability improvement of wind turbine penetrated using power system stabilizer (PSS) on South Sulawesi transmission system", *AIP Conference Proceedings*, Vol. 1941, No. 1, p. 020036, 2018, doi: 10.1063/1.5028094.

[10] H. P. Patel and A. T. Patel, "Performance evaluation of PSS under different loading condition", In: *Proc. of 2015 Global Conference on Communication Technologies (GCCT)*, pp. 281-284, 2015, doi: 10.1109/GCCT.2015.7342667.

[11] A. Stativă, M. Gavrilaş, and V. Stahie, "Optimal tuning and placement of Power System Stabilizer using Particle Swarm Optimization algorithm", In: *Proc. of 2012 International Conference and Exposition on Electrical and Power Engineering*, pp. 242-247, 2012, doi: 10.1109/ICEPE.2012.6463922.

[12] M. R. Djalal, M. Y. Yunus, H. Setiadi, and A. U. Krismanto, "Small-Signal-Stability Enhancement using a Power-System Stabilizer based on the Cuckoo-Search Algorithm against Contingency N-1 in the Sulselrabar 150-kV System", *Makara Journal of Technology*, Vol. 22, No. 1, pp. 1-8, 2018, doi: 10.7454/mst.v22i1.3497.

[13] S. Keskes, N. Bouchiba, S. Sallem, L. C. Alaoui, and M. B. A. Kammoun, "Optimal tuning of power system stabilizer using genetic algorithm to improve power system stability", In: *Proc. of 2017 International Conference on Green Energy Conversion Systems (GECS)*, pp. 1-5, 2017, doi: 10.1109/GECS.2017.8066200.

[14] A. Khodabakhshian and R. Hemmati, "Multi-machine power system stabilizer design by using cultural algorithms", *International Journal of Electrical Power & Energy Systems*, Vol. 44, No. 1, pp. 571-580, 2013, doi: 10.1016/j.ijepes.2012.07.049.

[15] H. Setiadi and K. O. Jones, "Power system design using firefly algorithm for dynamic stability enhancement", *Indonesian Journal of Electrical Engineering Computer Science*, Vol. 1, No. 3, pp. 446-455, 2016, doi: 10.11591/ijeecs.v1.i3.pp446-455.

[16] W. Peres, E. J. Oliveira, J. A. P. Filho, D. N. Arcanjo, I. C. Silva, and L. W. Oliveira, "Power system stabilizers tuning using bio-inspired algorithm", In: *Proc. of 2013 IEEE Grenoble Conference*, pp. 1-5, 2013, doi: 10.1109/PTC.2013.6652355.

[17] J. Kennedy and R. Eberhart, "Particle swarm optimization", In: *Proc. of ICNN'95-International Conference on Neural Networks*, Vol. 4, pp. 1942-1948, 1995.

[18] J. H. Holland, "Adaptation in natural and artificial systems", *An Introductory Analysis With Applications to Biology, Control, and Artificial Intelligence*, 1992.

[19] X. S. Yang, *Nature-inspired metaheuristic algorithms*, Luniver press, 2010.

[20] N. Mansouri, B. M. H. Zade, and M. M. Javidi, "Hybrid task scheduling strategy for cloud computing by modified particle swarm optimization and fuzzy theory", *Computers Industrial Engineering*, Vol. 130, pp. 597-633, 2019, doi: 10.1016/j.cie.2019.03.006.

[21] H. Zhou, J. Pang, P. K. Chen, and F. D. Chou, "A modified particle swarm optimization algorithm for a batch-processing machine scheduling problem with arbitrary release times and non-identical job sizes", *Computers Industrial Engineering*, Vol. 123, pp. 67-81, 2018, doi: 10.1016/j.cie.2018.06.018.

[22] J. Chen and J. Shi, "A multi-compartment vehicle routing problem with time windows for urban distribution–A comparison study on particle swarm optimization algorithms", *Computers Industrial Engineering*, Vol. 133, pp. 95-106, 2019, doi: 10.1016/j.cie.2019.05.008.

[23] H. Saadat, *Power System Analysis*, McGraw-Hill, 2009.

[24] P. S. Kundur and O. P. Malik, *Power system stability and control*, McGraw-Hill Education, 2022.

[25] Z. M. Gao, J. Zhao, S. R. Li, and Y. R. Hu, "The improved mayfly optimization algorithm", *Journal of Physics: Conference Series*, Vol. 1684, p. 012077, 2020, doi: 10.1088/1742-6596/1684/1/012077.